Dynamics of Premixed Hydrogen/Air Flames in Unsteady Flow

F. Zhang*,[1,2] T. Zirwes,[3,2,4] Y. Wang,[5] Z. Chen,[5] H. Bockhorn,[2] D. Trimis,[2] and D. Stapf[1]

[1)] *Institute for Technical Chemistry, Karlsruhe Institute of Technology, Karlsruhe Hermann-von-Helmholtz-Platz 1, Germany.*

[2)] *Engler-Bunte-Institute, Division of Combustion Technology, Karlsruhe Institute of Technology, Engler-Bunte-Ring 1, 76131 Karlsruhe, Germany.*

[3)] *Steinbuch Centre for Computing, Karlsruhe Institute of Technology, Hermann-von-Helmholtz-Platz 1, Karlsruhe, Germany.*

[4)] *Department of Mechanical Engineering, Stanford University, Stanford, CA 94305*

[5)] *College of Engineering, Peking University, Beijing 100871, China.*

(*Electronic mail: feichi.zhang@kit.edu)

(Dated: 5 July 2022)

Fully resolved numerical simulations with finite rate chemical reactions and detailed molecular diffusion have been conducted for a series of laminar premixed hydrogen-air flames under atmospheric condition. Objective of the work is to study the influence of unsteadiness of the flow on the local and global flame dynamics. Two equivalence ratios with $\Phi = 0.5$ and $\Phi = 4$ are considered, leading to a negative and a positive Markstein number Ma^0 at steady-state condition. The flames are excited with oscillating inflows at pre-defined frequencies f to assess the effect of unsteady flame stretch on flame dynamics. The Damköhler number, defined by the ratio of the inverse frequency of the oscillations and flame transit time, is used to characterize the interactions between the flow and the chemical reactions based on their time scales. For both lean and rich flame conditions, the local flame speed S_l is less sensitive to the flame stretch in an unsteady flow, which results in a reduced magnitude of the Markstein number $|\widetilde{Ma}|$. In addition, $|\widetilde{Ma}|$ is smallest when the time scale of the flow approaches the intrinsic time scale of the flame ($Da \approx 1$).

The global consumption speed S_t, computed from integration of the fuel burning rate over the whole computational domain, yields a phase delay and a damped oscillation with respect to the unsteady inflow: the phase delay increases with f or decreasing Da, whereas the reverse trend has been found for the oscillation amplitude of S_t. The flame is not able to follow the unsteady flow or adjust its flame surface at high excitation frequencies with $Da < 1$, and vice versa in the low frequency range with $Da \gg 1$. An efficiency factor E has been introduced to model the damped response of the flame due to flow unsteadiness, which reproduces the asymptotic behavior of $E \to 0$ at $Da \ll 1$ and $E \to 1$ at $Da \gg 1$. The simulation results reveal that the fluctuation time scale plays a significant role in elucidating the effect of flame-flow interaction, which should be considered for turbulent combustion modeling.

This work is dedicated to Prof. Pfitzner for his excellent and impressive scientific achievements in the field of modeling and analyzing turbulent combustion processes.

I. INTRODUCTION

Turbulent premixed combustion is controlled by flame-turbulence interactions leading to changes in local and global flame dynamics and consumption rates. The flame surface is stretched by tangential straining and/or curvature caused by the non-uniform, unsteady flow, altering the internal flame structure as well as the local and global burning rate of fuel. At high pressures, the flame becomes thinner and highly turbulent fluctuations may lead to flame wrinkles with extremely large curvatures and flame stretch. Accordingly, the classic flamelet approach, which employs stationary laminar unstretched flames for representing the turbulent flame structure, is not suited in this case.

The flame dynamics in terms of the correlation between laminar or turbulent flame speed with flow stretch has been extensively studied in the last decades[1–10]. Most of these works were focused on analyzing single snapshots (e.g. for spherically expanding flames) or time-mean flame structures (e.g. for Bunsen-type flames), which assign the influence of flame stretch to integral properties such as the turbulent length scale L_t or the root mean square (rms) values of the velocity fluctuations u'. Therewith, the time history of the unsteady flow and its effect on the flame dynamics have been neglected. However, as shown in[11] by detailed numerical simulation of oscillatory plane-jet H_2/air flames, the flame displacement is attenuated strongly in an unsteady flow, particularly in the high-frequency range of fluctuations. The flame requires a relaxation time to adapt to the imbalance of the prevailing diffusion-reaction processes caused by the unsteady flow. Similar behavior has been reported in[8,9,12] applying direct numerical simulation (DNS) of 1D counter-flow oscillating, premixed H_2/air flames and 3D turbulent methane/air flames[1]. It has been shown in the latter case that motion of the flame surface was weakened at fluctuation frequencies above the inverse of the flame transit time $\tau_c = \delta_l^0 / S_l^0$ defined by the ratio of unstretched laminar flame thickness δ_l^0 and unstretched laminar flame speed S_l^0. Therefore, the time scale of the flow represents an essential parameter for studying the effect of flame-turbulence interactions, which should be considered in addition to L_t and u'. For studying the effect of the flow time scale on flame-turbulence interactions, it is regarded as the oscillation period of the velocity fluctuation and is normalized by the chemical time scale to obtain the Damköhler number $Da = \tau_t / \tau_c$.

Although implicitly including an integral turbulent time

scale via $\tau_t = L_t/u'$, present models are not able to predict the observed effect of flow unsteadiness on flame dynamics due to incomplete consideration of the underlying flow history. Instead, most of the available combustion models assume the fast chemistry limit with $Da \gg 1$, i.e. the instantaneous adaption of the chemical reactions to the unsteady flow. Therefore, objective of the current work is to explore the effect of unsteady stretch on the local and global flame dynamics, which could be incorporated into general combustion modeling concepts. For that purpose, detailed numerical simulations have been conducted for a variety of premixed Bunsen-type, hydrogen/air flames, being excited with harmonically fluctuating inflow velocities at prescribed frequencies. The oscillating inflow is employed to emulate the unsteady nature of turbulent flow. Compared with the previous 1D studies conducted for 1D purely strained counter-flow flames[9], this work assesses quantitatively the local and global flame dynamics by means of the time-mean Markstein number and the global consumption speed. Moreover, the study is conducted for a more general 2D Bunsen-type flame setup, which covers both the tangential straining and curvature effects. In this way, correlations of the local and global flame speed with unsteadiness of the flow can be quantitatively assessed. The results can be used to derive first-order estimations for modeling the time history effect of the flow on premixed flame propagation.

The work is organized as follows: Sec.II presents basic parameters used in this work for characterizing flame dynamics in terms of flame speed and stretch. The numerical setups used for the simulations are shown in Sec.III. The simulation results are discussed in Sec.IV with respect to the flame's local and global dynamics. Finally, the main conclusions are summarized in Sec.V.

II. THEORETICAL BASICS

Flame dynamics describe the correlation between flame speed and flame surface area, which is controlled by the underlying reaction-diffusion processes during combustion. The flame surface can either be stretched tangentially through gradients of the flow velocity, and/or by the movement of a curved flame surface. By definition, the flame stretch K is calculated by means of the material derivative of a flame surface element, which can be rewritten identifying one part due to the aerodynamic strain K_S and another part due to flame propagation in its normal direction K_C[11]

$$K = K_S + K_C = a_T + S_d \kappa \tag{1}$$

S_d is the displacement speed, $\kappa = \nabla \cdot \vec{n}$ the flame surface curvature and $a_T = (I - \vec{n}\vec{n}) : \nabla \vec{u}$ the tangential strain rate with the unit tensor I. $\vec{n}$ is the unit surface normal vector pointing toward the fresh gas and $\vec{u}$ is the velocity vector. As a first-order estimate, the laminar flame speed S_l can be correlated linearly with the flame stretch[11]

$$\frac{S_l}{S_l^0} = 1 - MaKa \tag{2}$$

with the normalized stretch rate Ka

$$Ka = \frac{\delta_l^0}{S_l^0} K \tag{3}$$

and the Markstein number Ma

$$Ma = -\frac{\partial S_l / S_l^0}{\partial Ka} \tag{4}$$

In this way, Ma represents a measure of the sensitivity of S_l with respect to Ka or K. For $Ma > 0$, S_l decreases with Ka, and for $Ma < 0$, S_l increases with Ka.

In this work, the laminar flame speed is calculated from integration of the reaction rate of fuel $\dot{r}_F$ locally along the flame-normal direction

$$S_l = -\frac{1}{\rho_\mathrm{u}(Y_\mathrm{u} - Y_\mathrm{b})} \int \dot{r}_\mathrm{F} \mathrm{d}n \tag{5}$$

where ρ_u is the density of the unburnt mixture, Y_u and Y_b are the mass fractions of the fuel in the unburnt and burnt gas. In the same way, the global consumption speed S_t, corresponding to the overall burning rate or the bulk flow rate of fuel, has been evaluated from integration of $\dot{r}_\mathrm{F}$ over the entire computational domain

$$S_t = -\frac{1}{\rho_\mathrm{u}(Y_\mathrm{u} - Y_\mathrm{b})A_0} \int \dot{r}_\mathrm{F} \mathrm{d}V \tag{6}$$

where A_0 is a reference surface area, defined as the inlet area of the domain in the current work. In Eq.(5) and Eq.(6), both S_l and S_t are evaluated in terms of the consumption rate of fuel $\dot{r}_\mathrm{F}$ and indicate flame consumption speed in this work.

III. SIMULATION SETUP

A. Computational grid

Premixed hydrogen-air flames at the equivalence ratios of $\phi = 0.5$ and $\phi = 4$ are used in this work. The initial temperature and pressure are 300 K and 1 bar. Table I lists flame parameters calculated from solutions of 1D unstretched, freely propagating flames, which are used for setting up the simulations.

$$\delta_{th}^0 = \frac{\max(T) - \min(T)}{\max(\mathrm{grad}(T))} \quad \text{and} \quad \tau_c = \frac{\delta_{th}^0}{S_l^0} \tag{7}$$

are the thermal thickness of the flame and the flame transit time. $f_c = 1/\tau_c$ represents the intrinsic frequency of the flame. The flame front is identified by the iso-surface of the mass fraction of fuel Y_Iso shown in the last column of Tab.I, which corresponds to the largest reaction rate of fuel from the 1D laminar flame solutions.

As illustrated in Fig.1, the numerical simulations have been conducted for a Bunsen-type flame. The computational domain is built from a wedge with an opening angle of 3°, assuming axial symmetry for a laminar round-jet flame. Only

TABLE I. Flame parameters from solutions of 1D H_2/air flames.

ϕ	S_l^0 [m/s]	δ_{th}^0 [mm]	τ_c [ms]	f_c [Hz]	Y_{Iso}
0.5	0.54	0.42	0.78	1287	0.0018
4	1.72	0.44	0.26	3912	0.081

one computational cell is used in the circumferential direction, so that the simulation domain is essentially two-dimensional. Since the simulations are performed in the framework of OpenFOAM, a wedge-shaped domain is required for OpenFOAM to treat the governing equations in cylindrical coordinates. y and x indicate the streamwise and radial coordinates. The dimensions of the boundaries have been set as multiples of δ_{th}^0, as indicated in Fig.1. The domain length is set to be three times the flame height estimated from S_l^0 and u_{bulk} assuming a perfect conical flame. An equidistant grid is used for the simulations, which resolves the flame thickness with 20 cells with a grid resolution of $\Delta \approx 20\ \mu$m.

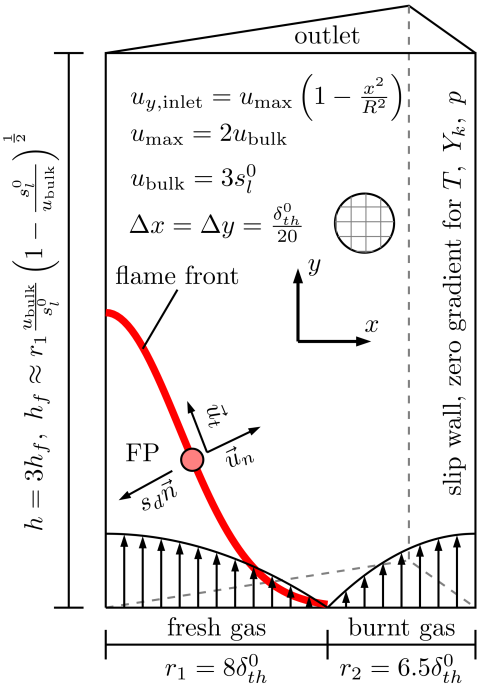

FIG. 1. Computational domain used for the simulation[13].

B. Boundary conditions

At the domain boundaries, premixed H_2/air enters the domain from the fresh gas inlet (bottom left) with a half-parabolic velocity profile

$$u_{y,\mathrm{inlet}} = u_{\max}(1-x^2/R^2) \tag{8}$$

where the maximum flow velocity at the centerline axis is set to $u_{\max} = 6S_l^0$ and the radius of the nozzle is R. This results in a bulk flow velocity of $u_{\mathrm{bulk}} = 3S_l^0$. The Reynolds numbers based on the bulk velocity and the inlet diameter are $Re = 577$ for $\phi = 0.5$ and $Re = 1032$ for $\phi = 4$. An annular coflow with fully burnt gas of the same mixture is used in order to stabilize the main flame. At the outlet boundary, gradients of all variables in the surface-normal direction are set to zero. The right boundary is set as a slip wall, along with vanishing gradients for the other quantities.

In order to study the effect of unsteady stretch on flame dynamics, the velocity profiles of the fresh and annular flow gases are excited to fluctuate harmonically in time with predefined frequencies f and a fixed amplitude $a = 0.5$:

$$u(t) = u_{y,\mathrm{inlet}}(1 + a\sin(2\pi f t)) \tag{9}$$

The Damköhler number defined by

$$Da = \frac{\tau_f}{\tau_c} = \frac{1/f}{1/f_c} = \frac{f_c}{f} \tag{10}$$

is used for characterization of the unsteady flame-flow interaction. f is selected for both lean and rich flames to span a wide range of Da from $Da < 1$ to $Da > 1$. The oscillation amplitude of the bulk inflow velocity and the diameter of the nozzle can be regarded as measures for the turbulence intensity and length scale of a general turbulent flow.

C. Numerical setups

The simulations have been carried out with an in-house solver developed in the framework of the open-source program OpenFOAM[14–16], which employs detailed calculations of the chemical reaction rates. The reaction mechanism developed by Li et al.[17] is used for hydrogen/air combustion. The chemical source terms are treated via an operator splitting approach, where the governing equations for batch reactors are integrated in each computational cell over the CFD simulation time step. Using the species concentrations in each cell at the beginning and at the end of the integration, a chemical source term that is averaged over the CFD time step can be computed and used as source term in the governing equations. A more detailed description of this procedure can be found in[14–16,18].

The mixture-averaged transport model is used to consider differential diffusion, with transport coefficients of each species computed from the Chapman-Enskog solution of kinetic gas theory. Soret and Dufour effects are not considered in this work. The latter one can generally be neglected as the contribution to the energy transport is negligible, even for hydrogen flames. As this paper focuses on very lean and rich hydrogen flames, the contribution of the Soret effect is less pronounced than at near-stoichiometric conditions. For example, the difference in laminar flame speed with and without Soret effect at $\phi = 1$ is about 11%, while the difference at $\phi = 4$ is 3% and at $\phi = 0.5$ is 6%. The solver has been validated in previous works[15,18–29]. The time steps are 0.5 μs for the $\phi = 0.5$ flame and 0.25 μs for the $\phi = 4$ flame, leading to a maximum convective CFL (Courant–Friedrichs–Lewy) number of 0.2 and a maximum Fourier number of 0.35.

A fully implicit scheme of second order accuracy for the time integration and a fourth order, unbounded interpolation scheme for discretization of the convective and diffusive terms have been used. The numerical solver employed in this work uses a pressure-velocity coupling via the PIMPLE (SIMPLE-PISO) algorithm. While this scheme is fully compressible in the sense of fully coupling density and pressure, it behaves more like a low Mach-number approach with regard to acoustics: Due to the implicit treatment and PIMPLE approach, the simulation time step is based on the convective CFL number number, not the acoustic CFL number. Therefore, acoustic waves are generally not resolved, since they are not the focus of this work. Instead, the non-reflective boundary at the outlet is used to prevent reflection in case of non-physical numerical oscillations. Additionally, a sponge region near the outlet avoids reflection of pressure waves back into the domain.

As the simulation is performed fully compressible, the oscillating mass flow at the inlet results in a fluctuation of the pressure inside the domain due to momentum conservation. The pressure fluctuation is particularly large in case of high excitation frequencies. However, as the amplitude of the oscillating mass flow and the length of the computational domain are small in this work, the maximum pressure variations observed in the computational domain are in the order of 100 Pa. Therefore, the effect of pressure on chemical reaction rates is negligible.

IV. RESULTS AND DISCUSSIONS

A. Overall flame structure

Figure 2 presents contours of calculated heat release rate $\dot{q}$ and temperature T from the steady-state solutions ($f = 0$ Hz) for $\phi = 0.5$ at the top and $\phi = 4$ at the bottom. The solid lines in the temperature fields on the right denote the flame fronts given by the iso-surfaces of Y_{Iso} (see Tab.I). For the rich flame with $\phi = 4$, $\dot{q}$ has a maximum at the flame tip and a minimum at the flame base. The behavior is however reversed for the lean flame with $\phi = 0.5$, where the flame is extinguished at the tip and $\dot{q}$ is largest at the flame base due to the high diffusivity of hydrogen: the flame is negatively curved at the flame tip, which results in a defocused diffusion of hydrogen from the fresh to the burnt side. Therefore, the local equivalence ratio ϕ_{Loc} is smallest at the flame tip, which leads to the highest $\dot{q}$ for the rich flame and the smallest $\dot{q}$ for the lean flame, as shown in Fig.3 by the contour-plots of ϕ_{Loc}, on the left for the $\phi = 0.5$ and on the right for the $\phi = 4$ flame. Due to the high diffusivity of hydrogen, ϕ_{Loc} is even smaller than that at the lower ignition limit for $\phi = 0.5$, so that the flame extinguishes at the flame tip. On the contrary, the flame yields the highest positive curvature at the flame base, which results in the largest ϕ_{Loc}. The correlation of heat release or burning rate with regard to flame curvature results in a negative Markstein number for the current lean flame (S_l increases with stretch) and a positive Markstein number for the considered rich flames (S_l decreases with stretch).

Figure 4 provides an overview of instantaneous contours

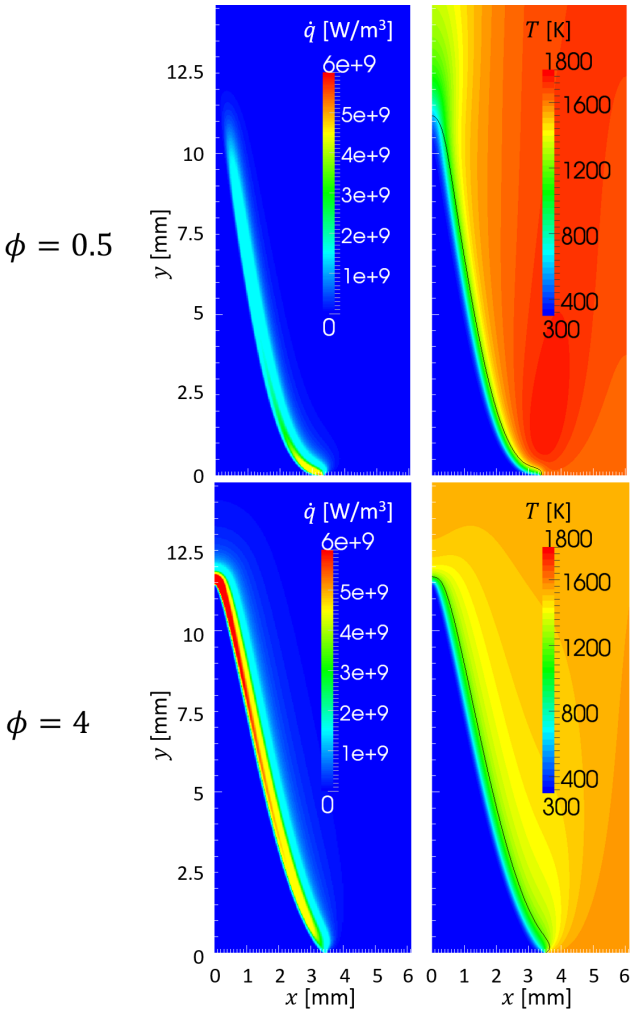

FIG. 2. Contours of heat release rate (left) and temperature (right) of steady-state H_2/air flames for $\phi = 0.5$ (top) and $\phi = 4$ (bottom).

of $\dot{q}$ calculated for the unsteady lean-premixed hydrogen-air flame at different f, where the flame shape deviates from that of the stationary flame shown in Fig.2. From left to right, four snapshots of $\dot{q}$ are used to represent one whole oscillation period for each Da, having a time interval of $T/4$ with $T = 1/f$. For the low frequency case with $f = 125$ Hz (see the first row with $Da \approx 10$ in Fig.4), the flame is able to adapt promptly to the oscillating inflow and moves periodically as a whole with a large displacement from its time-mean position. As f approaches the natural frequency of the flame (see the second and third rows with $Da = 2.5$ and $Da = 1$ in Fig.4), the flame enters a pulsating mode and becomes wrinkled. With further increased f (see the lowest row with $Da = 0.25$ in Fig.4), the flame turns into its steady-state solution without discernible motion. The same behavior with respect to flame response to unsteady flow has been found for the case with $\phi = 4$. Therefore, the overall flame response to an unsteady flow, in terms of changing its flame surface area through stretch, is attenuated with increased fluctuation frequency of the flow (see also Fig.7). This effect will be further elucidated in Sec.IV C.

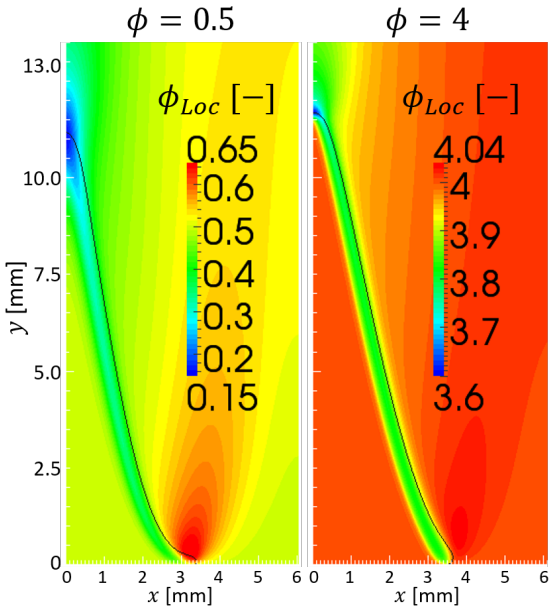

FIG. 3. Contours of calculated local equivalence ratio of steady-state H_2/air flames for $\phi = 0.5$ (left) and $\phi = 4$ (right).

B. Local flame dynamics and Markstein number

The flame particle (FP) method proposed in[13,30,31] has been applied in this work to assess the effect of unsteady flow on the local flame dynamics. The method introduces a number of virtual, massless particles along the flame surface and tracks them during flame propagation. In this way, the time evolution of each individual flame surface element along with variations of flow stretch conditions and burning rates can be recorded, allowing a detailed evaluation of the time history effect of the flow on the flame's local dynamics. Figure 5 plots S_l/S_l^0 against Ka for the $\phi = 0.5$ (top) and $\phi = 4$ (bottom) hydrogen/air flames, which are calculated from the FPs using Eq.(1) and Eq.(5). For the "on-the-fly" computation of S_l with Eq.(5), the line integration along the flame normal direction is performed locally over a distance of $1.5\delta_{th}^0$ on both sides of the flame surface. The black points indicate data obtained from the steady-state solutions, where S_l/S_l^0 increases with Ka for $\phi = 0.5$ and vice versa for $\phi = 4$. Therefore, the Markstein number for the stationary flames is negative for the lean flame and positive for the rich flame considered in this work. The flame is stabilized at the burner orifice and yields a radius of approx. 3 mm ($8\delta_{th}^0$). Therefore, cellular structures attributed to thermodiffusive instabilities cannot grow for the steady-state lean flame case with $\phi = 0.5$. For the oscillating lean flames, the corrugations on the flame surface are enhanced due to the thermodiffusive effect.

For the unsteady solutions plotted in Fig.5, the FPs are seeded at the base of the flame at a time distance of $T/8$ with $T = 1/f$. These FPs therefore follow different spatial trajectories in time and experience different stretch conditions. This leads to a scattering for the distributions of S_l/S_l^0 vs. Ka for the oscillating compared with the steady-state flames, as

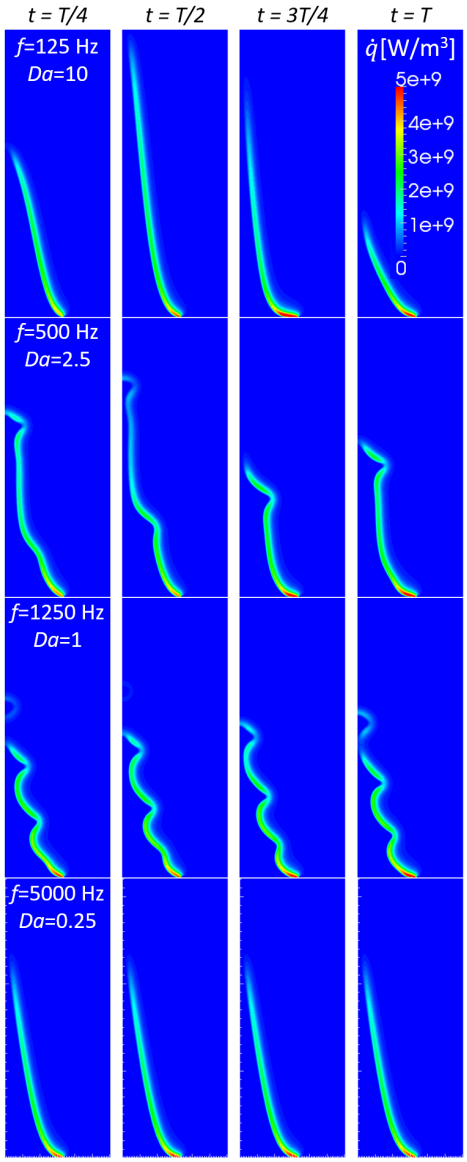

FIG. 4. Snapshots of calculated heat release rate of lean hydrogen/air flames at different excitation frequencies for $\phi = 0.5$.

shown in Fig.5. The diffusion-reaction balance prevailing the flame's local dynamics is disturbed by the unsteady velocity fluctuations. In this case, the flame requires a certain relaxation time for adjusting its internal structure and dynamics according to the transiently changing stretch, so that a previous state of S_l/S_l^0 is recorded by the FPs for the current Ka.

As shown in Fig.5, the scattering of $S_l/S_l^0(Ka)$ is particularly large when Da approaches unity ($Da \approx 1$). In contrary, $S_l/S_l^0(Ka)$ resembles the steady-state solutions for $Da < 1$ and $Da \gg 1$. The results indicate that the largest deviations of the local flame dynamics compared with that of the steady-state solution are due to the unsteady flow condition with $f \approx 1/\tau_c$ ($Da \approx 1$) or when the turnaround frequency of the flow approaches the flame's natural frequency. The internal structure of the flame sustained by the intrinsic reaction-diffusion bal-

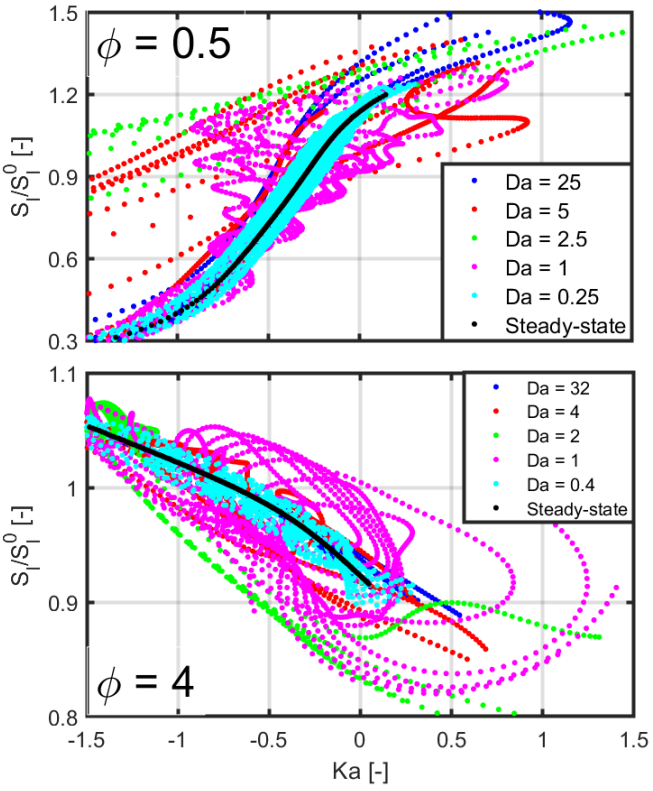

FIG. 5. Correlations of local consumption speed with normalized stretch rate calculated from detailed numerical simulations of oscillating hydrogen-air flames at $\Phi = 0.5$ (top) and $\Phi = 4$ (bottom).

ance yields the smallest resistance against external flow disturbances in this case, so that the flame is excited and falls into resonance with the unsteady flow fluctuations. Accordingly, the internal flame structure as well as the flame dynamics are altered considerably at $Da \approx 1$, which leads to enhanced wrinkling of the flame (see also Fig.4 for the case with $Da = 1$) and strong scattering of S_l/S_l^0 with respect to Ka.

Figure 6 plots the Markstein number $\overline{Ma}$ calculated from linear fitting of all data pairs of S_l/S_l^0 vs. Ka assigned to each excitation frequency shown in Fig.5. As the linear Markstein correlation is generally valid only for small stretch values with Ka close to 0, the fitting procedure has been performed for the range of $-1 < Ka < 1$. In this way, $\overline{Ma}$ corresponds to an unsteady or "turbulent" Ma averaged over different states of the flame during one oscillation period. The steady-state Markstein numbers Ma^0 used in the ordinate axis of Fig.6 for normalizing $\overline{Ma}$ are $Ma^0 = -0.78$ for $\phi = 0.5$ and $Ma^0 = 0.10$ for $\phi = 4$. $\overline{Ma}/Ma^0$ is less than unity in general under unsteady flow conditions, which indicates a decreased sensitivity of the local flame dynamics to stretch. The smallest values of $\overline{Ma}/Ma^0$ are found for Da close to unity, where the oscillation frequency matches with the flame's intrinsic frequency. The flame is excited and wrinkled in this case, as shown in the third row of Fig.4. Consequently, S_l/S_l^0 vs. Ka reveals a scattering in Fig.5. The correlation between S_l/S_l^0 and Ka is partly positive in the range of $-1 < Ka < -0.7$ for $\phi = 4$ due to formation of the enclosed envelope structures for S_l/S_l^0 and Ka, so that a significant decrease of $\overline{Ma}/Ma^0$ at $Da = 1$ can be detected in Fig.6 for this case.

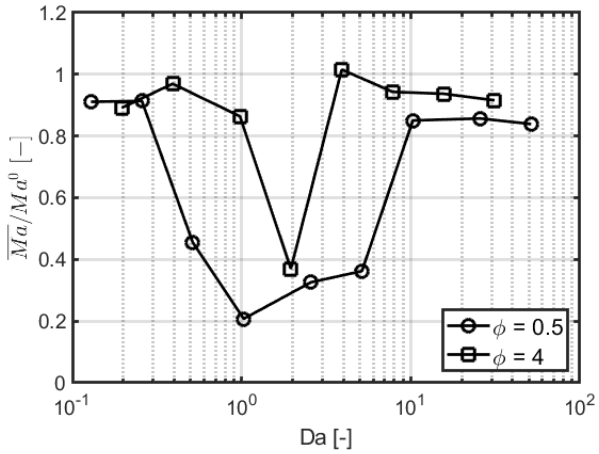

FIG. 6. Time-averaged Markstein numbers calculated from linear-fitting of data pairs of S_l/S_l^0 vs. Ka shown in Fig.5.

C. Global flame response to unsteady stretch

Figure 7 depicts the temporal evolution of the global consumption speed S_t calculated from integration of the fuel reaction rate over the whole domain, see Eq.(6). In this way, S_t corresponds to the bulk flow rate of fuel prescribed at the inflow, assuming a balance of incoming and consumed fuel mass. The time axis is normalized with the oscillation period $T = 1/f$ in order to compare S_t calculated from different excitation frequencies or Da. The dashed lines with a sinusoidal function in Fig.7 show the oscillation curve of the bulk inflow velocity u_{bulk}. S_t exhibits a phase delay $\Delta\alpha$ with respect to the inflow, as indicated in the lower part of Fig.7, which strictly increases with increasing f or decreasing Da. In addition, S_t yields a damped oscillation amplitude ΔS_t compared with that of the inflow. In the cases with $Da \leq 1$, the flame cannot respond to the highly unsteady flow and approaches its stationary solution, so that ΔS_t is decreased significantly and approaches 0. Figure 7 reveals that the ability of the flame to follow the flow fluctuation is strongly attenuated under the conditions of $Da \leq 1$. In this case, the oscillation amplitude of S_t is significantly weakened, but the time periods remain as given by $T = 1/f$.

The same behavior is illustrated in the phase diagram in Fig.8, where S_t (solid curves in Fig.7) is plotted against u_{bulk} (dashed curves in Fig.7). The delayed response of global flame dynamics in terms of S_t to the unsteady inflow results in a hysteresis loop with a tilted elliptical shape. At the same time, the oscillation amplitude of S_t is reduced with decreasing Da or increasing f, which is close to 0 for $Da \leq 1$ (quasi-horizontal curves in Fig.8). The results reveal that the overall flame dynamics are sensitive to flow stretch only at low excitation frequencies, whereas its response to the flow is strongly

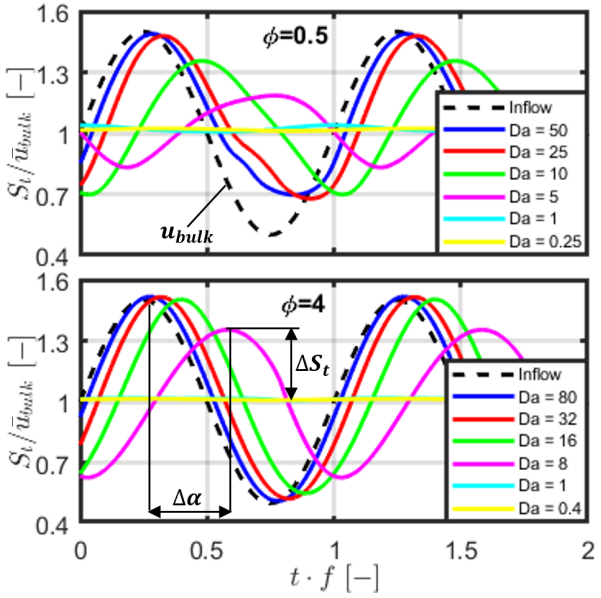

FIG. 7. Time developments of global consumption speeds calculated from simulations of oscillating hydrogen/air flames at different forcing frequencies.

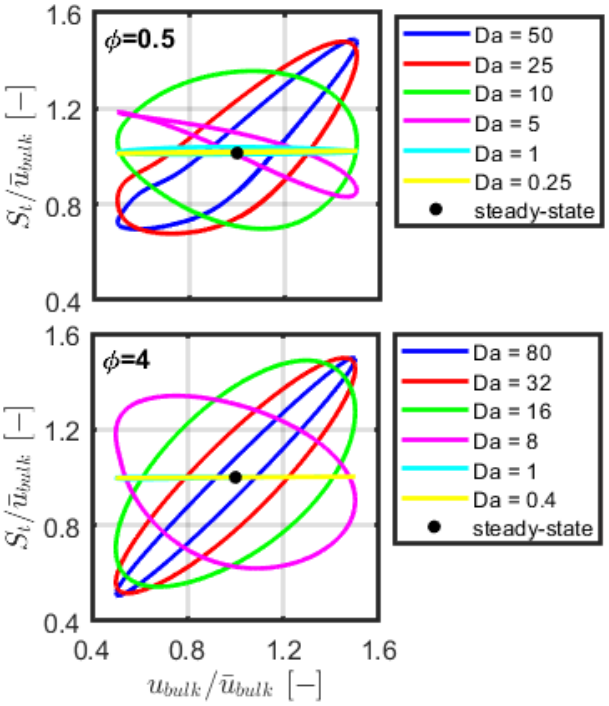

FIG. 8. Global consumption speed S_t plotted against the inflow bulk velocity at different Da.

attenuated in case of high frequencies.

In summary, the flame wrinkling or enlargement of flame surface caused by turbulent flow is mainly attributed to unsteady fluctuations with $Da > 1$. The flame regime "ideally stirred reactor" proposed in the classic Borghi-Peters regime diagram for $Da < 1$ and $Re_t > 1$, which is characterized by a considerably thickened flame brush and homogeneously mixed chemical state, is not visible.

D. Correlation of global consumption speed with total flame surface area

Figure 9 depicts S_t/S_l^0 as a function of the total flame surface area A_t/A_0, where A_0 is the area of the inlet boundary and the black dots represent the steady-state solutions. The solid line indicates the flamelet relation with $S_t/S_l^0 = A_t/A_0$, assuming that the local consumption speed S_l is equal to the unstretched laminar flame speed S_l^0. Although not shown here, A_t oscillates in a similar way as S_t in time (as shown in Fig.7) and no distinct phase delay between A_t and S_t has been observed. Therefore, S_t/S_l^0 and A_t/A_0 yield a quasi-linear correlation in Fig.9, but deviate from equality. The result reveals that the increase in S_t is due to the increase of A_t and almost not affected by the unsteady nature of the flow.

S_t/S_l^0 is larger for $\phi = 0.5$ than that for $\phi = 4$ at constant A_t/A_0, therefore, the stretch factor I

$$I = \frac{S_t/S_l^0}{A_t/A_0} \cong 1 - Ma \cdot Ka_t \tag{11}$$

which represents a measure for the normalized flame speed averaged over the whole flame surface, is larger for the lean

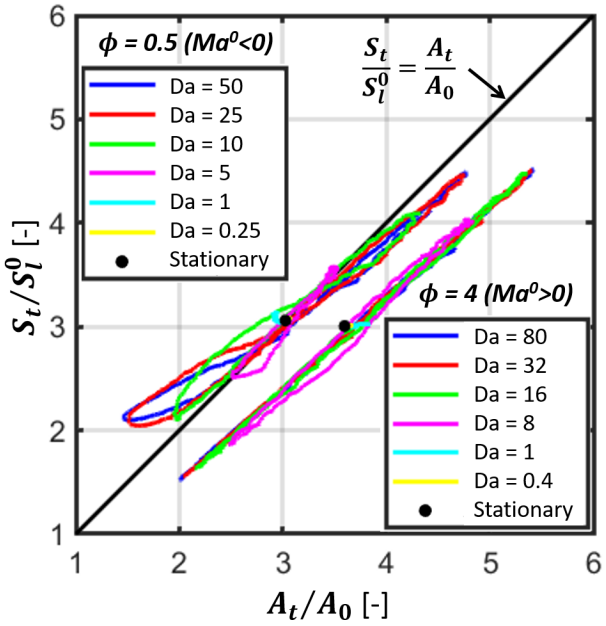

FIG. 9. Global consumption speed plotted against the total flame surface area of oscillatory H_2/air premixed flames at different Da.

flame. The reason is that Ma is negative for the $\phi = 0.5$ and positive for the $\phi = 4$ premixed hydrogen flame (see Fig.5), so that the local flame speed increases with Ka for the lean flame and vice versa for the rich flame.

The current round-jet flame experiences an overall high negative stretch due to curvature in the circumferential direc-

tion, which is compensated by the positive stretch component due to tangential straining, see Eq.(1). For the $\phi = 0.5$ flame, S_t/S_l^0 over A_t/A_0 in Fig.9 lies closely together with the reference curve (solid line) with $I \approx 1$, indicating that the global stretch Ka_t considering both curvature and straining of the whole flame surface is close to 0. In the case with $\phi = 4$, the bulk flow velocity at the inlet ($u_{\text{bulk}} = 3S_L^0$, see Sec.III and Tab.I) is much higher than that of the $\phi = 0.5$ flame. Therefore, the rich flame yields overall a positive Ka_t due to the higher positive tangential strain compared with the negative stretch caused by flame curvature. This leads to $I < 1$ according to $Ma > 0$ for the case with $\Phi = 4$. As a result, the correlation curves of S_t/S_l^0 vs. A_t/A_0 in Fig.9 lie below the reference line indicated with $S_t/S_l^0 = A_t/A_0$. Note that as the lean flame with $\phi = 0.5$ is locally extinguished at its tip (see Fig.2 and Fig.4), the flame surface area evaluated from the iso-surface of Y_{Iso} is overestimated. As a consequence, the distributions of S_t/S_l^0 vs. A_t/A_0 in Fig.9 for the lean flame should be shifted towards smaller A_t/A_0, which results in an increased I. As a conclusion, the averaged flame speed over the flame surface area is larger than S_l^0 in case of $Ma < 0$ and smaller than S_l^0 for flames with $Ma > 0$, which is valid for both stationary and transient flames.

E. Efficiency of flame response to unsteady stretch

In order to assess the damping effect on the fluctuation amplitudes of S_t or A_t caused by flow unsteadiness (see Fig.7 and Fig.8), an efficiency factor E is introduced as the ratio of the standard deviations of the time evolution of S_t and u_{bulk} shown in Fig.7

$$E = \frac{\text{std}(S_t)}{\text{std}(u_{bulk})} = \frac{S_t'}{u'} \tag{12}$$

which is used to quantify the effectiveness of flow stretch in altering global flame dynamics in an unsteady way. Assuming that the computational domain is represented by one control volume, E reflects the ability of the flame to increase its flame surface area or the mean reaction rate within the corresponding finite volume caused by unsteady flow fluctuations. E is plotted in Fig.10 against Da. The correlations of E with Da show a similar course for both lean and rich flames: E is close to 0 at $Da \to 0$, where the flame cannot respond to the high frequency fluctuations of the flow; with further increase of Da or decrease of f, E increases continuously until the asymptotic limit with $E \to 1$ or $S_t' = u'$, characterizing the flamelet regime, is reached at $Da \gg 1$.

In the literature, most of the available correlations for turbulent flame speed have been solely based on the turbulence intensity or u', which assumes the fast chemistry limit with $Da \gg 1$. The turbulent flame speed closure (TFC) model proposed by Schmid et al.[32] has been derived analytically based on a weighted time scale concerning the chemical and turbulence time scales, which reproduces the asymptotic limits with $S_t' \to 0$ at $Da \to 0$ and $S_t' \to u'$ at $Da \to \infty$. As the same behavior has been confirmed in the current simulations, the Schmid model has been used as a reference model to discuss the influence of Da on the overall burning rate. It expresses the turbulent flame speed $\hat{S}_t$ explicitly as a function of the turbulent Da or Da_t

$$\hat{S}_t = S_l^0 + u' \left(1 + Da_t^{-2}\right)^{-\frac{1}{4}},\ Da_t = \frac{\tau_t}{\hat{\tau}_c} \tag{13}$$

where the chemical time scale $\hat{\tau}_c$ is calculated with the thermal diffusivity of the fresh gas mixture a_0 and S_l^0.

$$\hat{\tau}_c = \frac{C_w^2}{C_e}\frac{a_0}{S_l^0 S_l^0},\ C_w = 2.4,\ C_e = 0.09 \tag{14}$$

Assuming $\hat{S}_t' = \hat{S}_t - S_l^0$, which indicates the contribution of flame speed fluctuations due to the turbulent flow, Eq.(13) can be reformulated to

$$\hat{E} = \frac{\hat{S}_t - S_l^0}{u'} = \frac{\hat{S}_t'}{u'} = \left(1 + Da_t^{-2}\right)^{-1/4} \tag{15}$$

which renders the effect of flow unsteadiness or Da_t on $\hat{S}_t$ and is shown in Fig.10 by the dashed curves. The asymptotic limits with $E \to 0$ at $Da \to 0$ and $E \to 1$ at $Da \to \infty$ have been reproduced by the Schmid model. However, E in the intermediate range with $0 < Da < 10$ is largely overestimated by the Schmid model compared with the results from this work. Despite these differences, the TFC model according to Eq.(13) has been applied successfully to simulate a number of turbulent premixed flames[33–35]. The reason is that the considered flame setups in these works are subjected to a large Da, so that the flame response to the turbulent flow in terms of $E = 1$ was correctly reproduced.

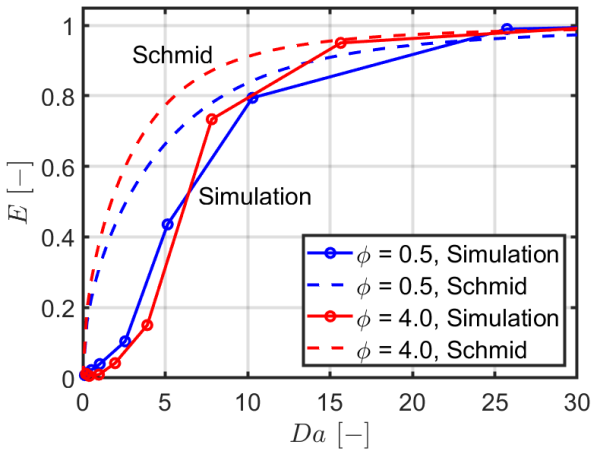

FIG. 10. Efficiency factor considering the effect of flame response to unsteady stretch in dependence of Da.

According to the results shown in Fig.10, the flame can follow the flow fluctuations and change its flame surface area only under the conditions of $Da > 10$ with $E > 80\%$; the ability of the flame to respond to velocity fluctuations is strongly weakened for $Da < 1$ with $E < 5\%$. This behavior for the effectiveness of global flame response to unsteady flow is illustrated in Fig.11. The result suggests an extension

of the regime diagram for flame-turbulence interaction with the asymptotic transition from a strongly responsive flame at $Da > 10$ to a weakly responsive flame at $Da < 1$ by a given turbulent Reynolds number. Its influence is particularly important in highly unsteady turbulent flows, where the energy cascade covers a wide range of time scales or Da. In this case, the flamelet correlation assuming a proportional increase of S_t with u' ($S_t = u'$) is strongly violated due to $Da < 1$. In addition, even an excessively large stretch rate will not lead to flame quenching at $Da < 1$, because the flame is not able to sense the highly unsteady flow stretch.

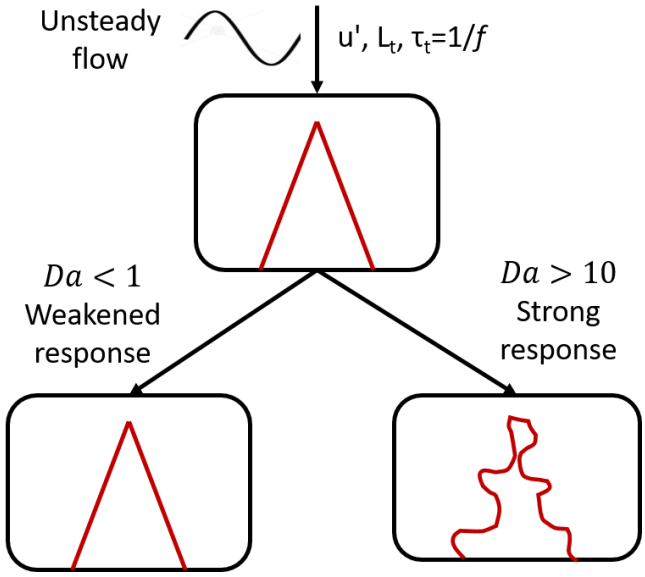

FIG. 11. Effectiveness of flame-turbulence interactions considering the influence of flow unsteadiness in terms of Da.

F. Discussion

The current work has reproduced the existing findings from the previous studies by Im and Chen[9] applied to 1D oscillating counter-flow flames, where the flame speed has been shown to be less sensitive to stretch under unsteady flow conditions. In the current work, a round-jet flame setup is used, which leads to a substantially extended stretch range, considering both effects caused by tangential strain and curvature, and covering both negative and positive stretch. Furthermore, the global flame response in terms of the overall flame surface area is used here to evaluate the global flame dynamics, whereas the concept of flame surface is less meaningful for the planar flame setup. Therefore, the current work extends considerably the available knowledge based on 1D studies.

The obtained results can be incorporated into combustion modeling concepts in order to account for the time history effect on the response of global flame dynamics. For that purpose, a fitting function may be derived to model the correlation of E with Da shown in Fig.10, which can be used to evaluate a cell-averaged burning rate based on S_t, for instance, in the framework of a RANS (Reynolds-Averaged Navier-Stokes) or LES (Large Eddy Simulation) concept.

Note that Da yields a non-uniform distribution along the flame surface in a general turbulent flame: on one hand, the broadband fluctuations of the flow cause variation of the local turbulent time scale and on the other hand, the flame thickness and the flame speed can be changed locally by the turbulent flow, which results in a different chemical time scale. Furthermore, the flame-turbulence interactions take place over a wide range of time scales in a real turbulent flame, whereas a fixed forcing frequency is applied to interact with the flame in the current study.

V. CONCLUSIONS

Detailed numerical simulations have been performed for a series of oscillating premixed H_2/air flames with pre-defined frequencies f. The objective is to assess systematically the impact of flow unsteadiness on the local and global flame dynamics. The flame requires a relaxation time to respond to the oscillating flow, so that flame speed S_l is less responsive to stretch under unsteady conditions. The statement is valid for both lean- and rich premixed flames with oblique flow and strained and curved flame structure. As a result, the magnitude of the Markstein number $|\overline{Ma}|$ decreases in an unsteady flow. The flame is excited with an enhanced wrinkling and $|\overline{Ma}|$ is smallest when f approaches the natural frequency of the flame, i.e., $Da \approx 1$.

The global consumption speed S_t, which correlates almost linearly with the total flame surface area, exhibits a phase delay $\Delta\alpha$ and a reduced amplitude ΔS_t with respect to the oscillating inflow. $\Delta\alpha$ increases with f, whereas the reversed trend is found for ΔS_t. The damped oscillation of S_t due to flow unsteadiness has been modeled with an efficiency factor E in dependence of Da, which reveals the asymptotic limits with $E \to 0$ for $Da \to 0$ and $E \to 1$ for $Da \to \infty$.

In conclusion, the time history effect or unsteadiness of the flow plays an essential role for the correct description of local and global flame dynamics regarding flame-flow interaction. The generally used flamelet assumption is valid only for large Da, having $E > 0.8$ for $Da > 10$ in the current work. This work has focused on premixed hydrogen/air flames excited at fixed single frequencies. Further studies for additional fuel/air mixtures and considering the interactions between different flow time-scales are required to justify the general validity of the obtained results.

ACKNOWLEDGMENTS

The authors acknowledge the financial support by the Helmholtz Association of German Research Centers (HGF), within the research field MTET (Materials and Technologies for the Energy Transition), subtopic “Anthropogenic Carbon Cycle" (38.05.01). This work utilizes computing resources from the supercomputers Hawk at HLRS Stuttgart and HoreKa at SCC/KIT. The work leading to this publication

was supported by the PRIME programme of the German Academic Exchange Service (DAAD) with funds from the German Federal Ministry of Education and Research (BMBF).

[1] J. Chen and H. Im, "Correlation of flame speed with stretch in turbulent premixed methane/air flames," Proc. Combust. Inst. **27**, 819–826 (1998).

[2] M. Weiß, N. Zarzalis, and R. Suntz, "Experimental study of markstein number effects on laminar flamelet velocity in turbulent premixed flames," Combust. Flame **154**, 671–691 (2008).

[3] P. Clavin, "Dynamic behavior of premixed flame fronts in laminar and turbulent flows," Prog. Energy Combust. Sci **11**, 1–59 (1985).

[4] J. Sinibaldi, C. Mueller, and J. Driscoll, "Local flame propagation speeds along wrinkled, unsteady, stretched premixed flames," Proc. Combust. Inst. **27**, 827–832 (1998).

[5] T. Echekki and J. Chen, "Unsteady strain rate and curvature effects in turbulent premixed methane-air flames," Combust. Flame **106**, 184–202 (1996).

[6] T. Echekki and J. Chen, "Analysis of the contribution of curvature to premixed flame propagation," Combust. Flame **118**, 308–311 (1999).

[7] T. Zirwes, F. Zhang, P. Habisreuther, J. Denev, and H. Bockhorn, "Response of local and global consumption speed to stretch in laminar steady-state flames," in *Proceedings of the European Combustion Meeting 2017* (2017).

[8] F. Egolfopoulos, "Dynamics and structure of unsteady, strained, laminar premixed flames," Proc. Combust. Inst. **25**, 1364–1373 (1994).

[9] H. Im and J. Chen, "Effects of flow transients on the burning velocity of laminar hydrogen/air premixed flames," Proc. Combust. Inst. **28**, 1833–1840 (2000).

[10] N. Fogla, F. Creta, and M. Matalon, "The turbulent flame speed for low-to-moderate turbulence intensities: Hydrodynamic theory vs. experiments," Combust. Flame **175**, 155–169 (2017).

[11] F. Zhang, T. Zirwes, P. Habisreuther, and H. Bockhorn, "Effect of unsteady stretching on the flame local dynamics," Combust. Flame **175**, 170–179 (2017).

[12] C. Law and C. Sung, "Structure, aerodynamics, and geometry of premixed flamelets," Prog. Energy Combust. Sci. **26**, 459–505 (2000).

[13] T. Zirwes, F. Zhang, Y. Wang, P. Habisreuther, J. Denev, Z. Chen, H. Bockhorn, and D. Trimis, "In-situ flame particle tracking based on barycentric coordinates for studying local flame dynamics in pulsating bunsen flames," Proc. Combust. Inst. **38(2)**, 2057–2066 (2021).

[14] F. Zhang, H. Bonart, T. Zirwes, P. Habisreuther, H. Bockhorn, and N. Zarzalis, "Direct numerical simulation of chemically reacting flows with the public domain code openfoam," in *High Performance Computing in Science and Engineering '14*, edited by W. Nagel, D. Kröner, and M. Resch (Springer Berlin Heidelberg, 2015) p. 221–236.

[15] T. Zirwes, F. Zhang, J. Denev, P. Habisreuther, and H. Bockhorn, "Automated Code Generation for Maximizing Performance of Detailed Chemistry Calculations in OpenFOAM," in *High Performance Computing in Science and Engineering '17*, edited by W. Nagel, D. Kröner, and M. Resch (Springer, 2017) pp. 189–204.

[16] T. Zirwes, F. Zhang, P. Habisreuther, M. Hansinger, H. Bockhorn, M. Pfitzner, and D. Trimis, "Quasi-DNS dataset of a piloted flame with inhomogeneous inlet conditions," Flow Turbul. Combust. **104**, 997–1027 (2020).

[17] J. Li, Z. Zhao, A. Kazakov, and F. Dryer, "An upyeard comprehensive kinetic model of hydrogen combustion," Int. J. Chem. Kinet. **36**, 566–575 (2004).

[18] T. Zirwes, F. Zhang, J. Denev, P. Habisreuther, H. Bockhorn, and D. Trimis, "Improved Vectorization for Efficient Chemistry Computations in OpenFOAM for Large Scale Combustion Simulations," in *High Performance Computing in Science and Engineering '18*, edited by W. Nagel, D. Kröner, and M. Resch (Springer, 2018) pp. 209–224.

[19] X. Wen, T. Zirwes, A. Scholtissek, H. Böttler, F. Zhang, H. Bockhorn, and C. Hasse, "Flame structure analysis and composition space modeling of thermodiffusively unstable premixed hydrogen flames–Part I: Atmospheric pressure," Combust. Flame **238**, 111815 (2021).

[20] X. Wen, T. Zirwes, A. Scholtissek, H. Böttler, F. Zhang, H. Bockhorn, and C. Hasse, "Flame structure analysis and composition space modeling of thermodiffusively unstable premixed hydrogen flames–Part II: Elevated pressure," Combust. Flame **238**, 111808 (2021).

[21] X. Chen, Y. Wang, T. Zirwes, F. Zhang, H. Bockhorn, and Z. Chen, "Heat release rate markers for highly stretched premixed CH4/air and CH4/H2/air flames," Energy Fuels **35**, 13349–13359 (2021).

[22] T. Zirwes, F. Zhang, P. Habisreuther, M. Hansinger, H. Bockhorn, M. Pfitzner, and D. Trimis, "Identification of flame regimes in partially premixed combustion from a quasi-dns dataset," Flow Turbul. Combust. **106**, 373–404 (2021).

[23] T. Zirwes, T. Häber, F. Zhang, H. Kosaka, A. Dreizler, M. Steinhausen, C. Hasse, A. Stagni, D. Trimis, R. Suntz, and H. Bockhorn, "Numerical Study of Quenching Distances for Side-wall Quenching Using Detailed Diffusion and Chemistry," Flow Turbul. Combust. **106**, 649–679 (2020).

[24] T. Zirwes, F. Zhang, T. Häber, and H. Bockhorn, "Ignition of combustible mixtures by hot particles at varying relative speeds," Combust. Sci. Technol. **191**, 178–195 (2019).

[25] T. Häber, T. Zirwes, D. Roth, F. Zhang, H. Bockhorn, and U. Maas, "Numerical simulation of the ignition of fuel/air gas mixtures around small hot particles," Z. Phys. Chem. **231**, 1625–1654 (2017).

[26] F. Zhang, T. Zirwes, T. Häber, H. Bockhorn, D. Trimis, and R. Suntz, "Near Wall Dynamics of Premixed Flames," Proc. Combust. Inst. **38**, 1955–1964 (2021).

[27] Y. Wang, H. Zhang, T. Zirwes, F. Zhang, H. Bockhorn, and Z. Chen, "Ignition of dimethyl ether/air mixtures by hot particles: Impact of low temperature chemical reactions," Proc. Combust. Inst. **38**, 2459–2466 (2021).

[28] T. Zirwes, F. Zhang, J. Denev, P. Habisreuther, H. Bockhorn, and D. Trimis, "Implementation of Lagrangian Surface Tracking for High Performance Computing," in *High Performance Computing in Science and Engineering '20*, edited by W. Nagel, D. Kröner, and M. Resch (Springer, 2020).

[29] F. Zhang, T. Zirwes, P. Habisreuther, and H. Bockhorn, "A DNS Analysis of the Evaluation of Heat Release Rates from Chemiluminescence Measurements in Turbulent Combustion," in *High Performance Computing in Science and Engineering '16*, edited by W. Nagel, D. Kröner, and M. Resch (Springer, 2016) pp. 229–243.

[30] S. Chaudhuri, "Life of flame particles embedded in premixed flames interacting with near isotropic turbulence," Proc. Combust. Inst. **35**, 1305–1312 (2015).

[31] T. Zirwes, F. Zhang, and H. Bockhorn, "Memory effects of local flame dynamics in turbulent premixed flames," in *Combustion Symposium (internat.)*, Vol. 39 (2022).

[32] H. Schmid, P. Habisreuther, and W. Leuckel, "A model for calculating heat release in premixed turbulent flames," Combust. Flame **113**, 79–91 (1998).

[33] F. Zhang, P. Habisreuther, H. Bockhorn, H. Nawroth, and C. Paschereit, "On prediction of combustion generated noise with the turbulent heat release rate," Combust. Sci. Technol **99(6)**, 940–951 (2013).

[34] F. Zhang, T. Zirwes, P. Habisreuther, H. Bockhorn, D. Trimis, H. Nawroth, and C. Paschereit, "Impact of combustion modeling on the spectral response of heat release in les," Acta Acust united Ac. **191(9)**, 1520–1540 (2019).

[35] F. Zhang, T. Zirwes, P. Habisreuther, N. Zarzalis, H. Bockhorn, and D. Trimis, "Numerical simulations of turbulent flame propagation in a fan-stirred combustion bomb and bunsen-burner at elevated pressure," Flow Turbul. Combust **106**, 925–944 (2021).